Journal of Sound and Vibration 329 (2010) 3999–4016

Contents lists available at ScienceDirect

Journal of Sound and Vibration

journal homepage: www.elsevier.com/locate/jsvi

Identification of substructure properties of railway tracks by dynamic stiffness measurements and simulations

Eric G. Berggren [a,*], Amir M. Kaynia [b], Björn Dehlbom [c]

[a] Swedish National Rail Administration, Technical Department, 781 85 Borlänge, Sweden
[b] Norwegian Geotechnical Institute (NGI), P.O. Box 3930 Ullevål Stadion, 0806 Oslo, Norway
[c] Ramböll, Box 1932, 791 19 Falun, Sweden

ARTICLE INFO

Article history:
Received 17 April 2009
Received in revised form
13 April 2010
Accepted 15 April 2010
Handling Editor: M.P. Cartmell
Available online 10 May 2010

ABSTRACT

A new vehicle has been developed to measure dynamic vertical track stiffness while in motion. This technique allows the resonance behaviour of the track below 50 Hz to be measured. Soft soils like clay and peat are the main causes of resonance below 20 Hz. By means of simulation studies with the software *VibTrain*, soft soil resonance behaviour may be characterized using a few key parameters originating from track stiffness measurements, such as the minimum phase delay and corresponding frequency of the receptance transfer function. Statistical models are built to relate these key parameters with substructure properties, such as embankment thickness, shear wave velocity and thickness of the soft soil layer using pattern recognition methods. Two case studies are used to show the methodology, and the results are verified using Ground Penetration Radar (GPR) measurements and borehole investigations. Models are also developed from the statistical relationship between GPR-data and stiffness measurements. It is shown that embankment thickness is the easiest quantity to estimate, but indicative results are also presented for the other quantities (shear wave velocity and thickness of soil layer).

1. Introduction

Railway lines are investments with very long life and many tracks are over 100 years old. Although many components are replaced with time, some remain unchanged—especially the substructure. Soft soils, such as peat and clay, often introduce problems because the requirements for track performance today are different from those when the tracks were originally constructed. There is a clear trend towards higher speeds and increased capacity (i.e. more and heavier trains on the tracks). In order to deal with these changing circumstances, there is a focus on both condition assessment and track maintenance to ensure safety, comfort, availability and economy. Soft soils are often the source of problems related to bearing capacity, ground-borne vibrations, stability, settlements and track geometry irregularities. Unfortunately, condition assessment of the railway substructure is not a simple task due to inaccessibility. Site investigations using excavations or boreholes provide direct evidence of substructure status, but are impossible to perform continuously along the track. There are a few methods for continuous substructure condition assessment [1,2] of which Ground Penetrating Radar (GPR) is perhaps the most common. However, GPR can only provide information about certain aspects of the upper part of the substructure (like ballast and embankment thickness). There is therefore a need for new condition monitoring methods of railway track substructures. The EU research projects, Supertrack [3] and Innotrack [4] included the issue of condition assessment and parts of the current study were performed within this framework.

* Corresponding author. Tel.: +46 243 445658; fax: +46 243 445617.
E-mail address: eric.berggren@banverket.se (E.G. Berggren).

0022-460X/$ - see front matter © 2010 Elsevier Ltd. All rights reserved.
doi:10.1016/j.jsv.2010.04.015

There are different definitions of track substructure; this paper adopts the definition given by Selig and Waters [2], meaning all material beneath the sleeper, including the subsoil.

The outline of the paper is as follows: Section 1.1 presents a short description of the new tool for dynamic track stiffness measurements. Sections 1.2 and 1.3 include a short introduction to conceptual soft soil dynamics and excitation from trains. Section 2 describes a model developed in the simulation software *VibTrain*, and gives details of the parametric studies performed. Section 3 outlines the identification of substructure properties from stiffness measurements using both models constructed from the parametric studies, and GPR-measurements combined with site investigations. The methodology is demonstrated at two different sites in Section 4. Finally, conclusions are given in Section 5.

1.1. Track stiffness measurements

During recent years, several techniques for continuous measurement of vertical track stiffness have been developed, most notably in China [5], USA [6,7] and Sweden [8]. All of these methods, except the Swedish method, measure the static track stiffness. The Swedish Rolling Stiffness Measurement Vehicle (RSMV) can measure dynamic stiffness up to 50 Hz. The track is dynamically excited through two oscillating masses above an ordinary wheel axle of a freight wagon as shown in Fig. 1. The vertical track stiffness is calculated from the measured axle box forces and accelerations as described thoroughly in [8].

The RSMV can perform overall measurements at higher speeds (up to 60 km/h) with sinusoidal excitation, or detailed investigations at lower speeds (below 10 km/h) with noise excitation up to 50 Hz.

If the track structure does not contain soft soils, the difference between static and dynamic stiffness measurement methods is minor. As soft soils often have resonance behaviour at lower frequencies, a dynamic measurement will capture this to some extent depending on excited frequencies entailing differences between static and dynamic measurements. One other major difference is that a dynamic measurement will result in both the magnitude and the phase of the stiffness. Stiffness phase is rather non-explored from a practical point of view. This paper explores some of the stiffness phase interpretation and possible use.

Although continuous vertical stiffness measurements have been in use for a few years, there is still a lack of knowledge regarding how to interpret stiffness values, variation of stiffness along the track and the changing resonance behaviour of the track. The new RSMV is capable of exciting vibrations at the same low frequencies for which soft soils dramatically influence the track response. Therefore, there are possibilities for characterising the response of soft soils using the RSMV. Dynamic stiffness behaviour at higher frequencies is important when studying areas as corrugation growth, noise, train–track interaction forces, etc., though not covered by this study.

1.2. Approximate vertical resonance behaviour of railway tracks at lower frequencies (< 50 Hz)

In the following, two simplified descriptions of the low-frequency behaviour of railway tracks are given. Later a more advanced model will be used; however these simplified descriptions still give an engineering understanding of factors increasing/decreasing a low-frequency resonance of a railway track.

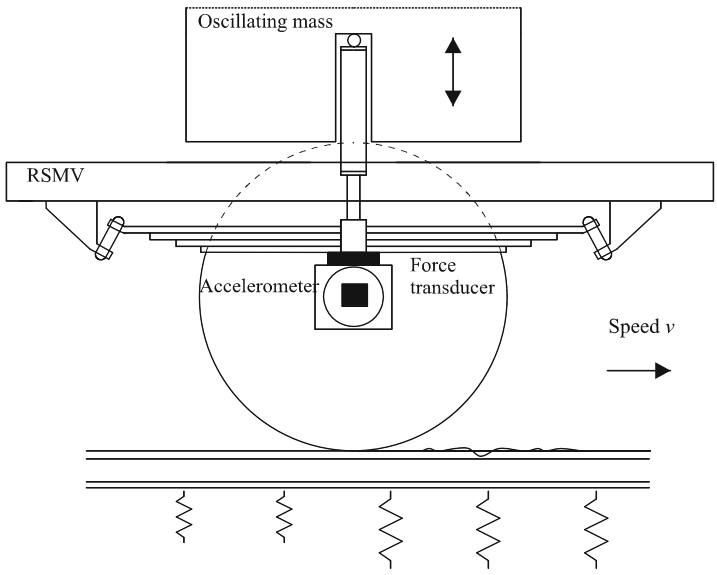

Fig. 1. Measurement principle (one side only) of RSMV [8].

Soft soils with low shear wave velocity (c_s) will show resonance behaviour at low frequencies. An approximate equation for the resonance frequency (f) is

$$f = \frac{c_s}{4H}(2n+1) \quad n = 0,1,2\ldots \tag{1}$$

where H is the depth of the soil layer [9]. For example, the first resonance frequency (n=0) of a 2 m deep clay layer with a shear wave velocity of 80 m/s will be only 10 Hz. The soil resonance behaviour will also be influenced by the overlying track structure. This can be conceptually understood by examining the resonance frequency of a simple single degree of freedom mechanical system described by the well-known equation:

$$f = \frac{1}{2\pi}\sqrt{\frac{k}{m}} \tag{2}$$

The soil stiffness is represented by the spring constant k and the track structure weight by the mass m. Softer clay (lower k) will result in a lower resonance frequency, as will a thicker embankment (higher m).

It is very difficult to analyse the vibration of ballast because of its granular configuration and special mechanism. Some advance has been made on dynamic modelling of the ballast [10–12]. Previous research suggests a first resonance frequency at 70–110 Hz. Work performed to investigate optimal performance of tamping machines [13] found that an elasto-liquid behaviour of the ballast occurs above 40 Hz. This may also be interpreted as a type of resonance.

1.3. Sources of dynamic train–track interaction at low frequencies (< 50 Hz)

There are several possibilities of coincidence between the low frequency behaviour of the track (especially tracks with soft soil substructures) and the frequency content due to a passing train. Unfortunate combinations can initiate ground-borne vibrations, thereby increasing the rate of degradation of the substructure resulting in greater need for maintenance.

The key factors determining the vertical low frequency content in the train–track interaction are the train (speed, axle distances, eigenmodes of vehicles, etc.) and the track (receptance and irregularities). The static rail deflection shape function, $d(x)$, under a wheelset can be described using the "beam on elastic foundation" model proposed by Zimmermann [1] as

$$d(x) = e^{-|x|L}\left(\cos\left(\frac{x}{L}\right) + \sin\left(\frac{|x|}{L}\right)\right) \tag{3}$$

x is the position along the track (wheelset at x=0) and L is the so-called characteristic length ($L = \sqrt[4]{4EI/k_f}$, EI is the bending stiffness of the rails and k_f is the foundation modulus), which is a measure of the track support quality. A longer characteristic length represents lower performance, for instance 1.3 m corresponds to poor track and 0.7 m to good track according to Esveld [1]. When travelling with a speed v, the correspondence of Eq. (3) will contain a dominating wavelength of $2\pi L$ metres. The equation can be repeated at distances corresponding to bogie and vehicle distances for each wheelset to arrange a whole train. Common distances between wheelsets in a train and the corresponding frequencies (f=v/λ) at different speeds are listed in Table 1.

In Table 1, the distance a corresponds to the *nearest* wheelset/bogie in an adjacent vehicle and b to the wheelset/bogie *at the same position* in an adjacent vehicle (same as vehicle length).

An example of sleeper deflections during a train passage at 170 km/h is shown in Fig. 2. The distance of wheelsets within each bogie is 2.9 m which is represented by time t_1 and frequency f_2. The distance of bogie pivots between adjacent vehicles is 7 m, which is indicated by time t_2 and frequency f_1. The vehicle length is indicated in the figure by time t_3. The vehicle length caused considerable vibrations at the site Ledsgård in Sweden [14]. This site had such a soft substructure before reconstruction (large L) that individual wheelsets or bogies could not be identified in sleeper deflection figures like Fig. 2a. The track response can be found in Fig. 5 (where it is used for verification of the simulation model). In this case, the track resonance (2.7 Hz) coincided with the train excitation for speeds close to 200 km/h [14].

As explained above, the track may experience resonance at low frequencies with a substructure containing soft soils and the train will excite the track at certain frequencies. Another important factor to train–track interaction at low

Table 1
Characteristic distances and frequency content from wheelsets during train passage.

	Wheelset L=1.3 m	Wheelset L=0.7 m	Wheelsets within bogie	Wheelsets between adjacent vehicles	Wheelsets within vehicle
Distance (λ)	8.1 m	4.4 m	1.5–3 m	*a*, 2–8 m; *b*, 15–30 m	7–20 m
Frequencies at v=100 km/h	3.4 Hz	6.3 Hz	9.3–19 Hz	*a*, 3.5–14 Hz; *b*, 0.9–1.9 Hz	1.9–5.0 Hz
Frequencies at v=200 km/h	6.9 Hz	13 Hz	19–37 Hz	*a*, 6.9–28 Hz; *b*, 1.9–3.7 Hz	3.7–10 Hz
Frequencies at v=300 km/h	10 Hz	19 Hz	28–56 Hz	*a*, 10–42 Hz; *b*, 2.8–5.6 Hz	5.6–15 Hz

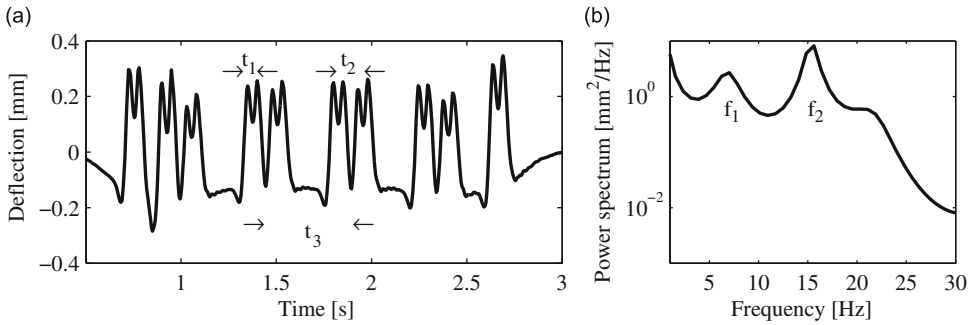

Fig. 2. Sleeper deflection during train passage with speed 170 km/h: (a) time domain and (b) frequency domain-power spectral density.

Table 2
Characteristic lengths and frequency contents from track irregularities and sleeper distance.

	Track irregularities 1–50 m (Hz)	Sleeper distance 0.5–0.7 m (Hz)
Frequencies at v=100 km/h	0.6–28	40–56
Frequencies at v=200 km/h	1.1–56	79–110
Frequencies at v=300 km/h	1.7–83	120–170

frequencies is the presence of track irregularities. Frequency contents from track irregularities, as well as sleeper distance, are listed in Table 2.

The track will directly experience the frequency content due to wheelset positions in the train (Table 1), but the train will only experience this if there are irregularities in the track. The train will directly experience the frequency content due to track irregularities and sleeper distance and the track will experience this as variations governed by the excitations of wheelsets.

2. Reference simulations

When measuring dynamic stiffness of tracks with soft soils, clear resonance behaviour can be found. However, it is not easy to interpret the results into physical properties such as shear wave velocity, thickness of embankment or thickness of soil layers. These physical properties may help to identify which soft zone cause problems to the infrastructure managers such as bearing capacity, vibration, or large track deflections. Therefore, simulations of different soils are proposed to support the interpretation of track stiffness measurements.

2.1. Theory of the simulation program VibTrain

Modelling and predicting railway vibration is an important field of research. Several authors have made major contributions, e.g. Clouteau et al. [15], Jones [16], Jones et al. [17], Krylov [18] and Madshus and Kaynia [19]. In this work, reference simulations are carried out using the software *VibTrain* [20–22]. Fig. 3 shows a general model for the software. The simulation model is based on a decomposition scheme whereby the track embankment structure is represented as a beam modelled by finite elements, and the ground is represented by Green's functions for a layered half-space. Despite the symmetry in structure and loading, the computational model is based on the full size of the track/soil.

The ground and embankment are considered as separate bodies under the nodal interaction forces. At a given excitation frequency ω, $\mathbf{P}$ denotes the vector of interaction forces between the ground and embankment and $\mathbf{W}$ represents the associated vector of vertical displacements, where these vectors can be related using the Green functions as

$$\mathbf{W} = \mathbf{G} \cdot \mathbf{P} \tag{4}$$

where $\mathbf{G}$ is a symmetric matrix with frequency-dependent complex entries G_{ij} defining the ground response at node i due to a unit load at node j. Inverting this relation, one can write

$$\mathbf{P} = \mathbf{G}^{-1}\,\mathbf{W} = \mathbf{K}_S \cdot \mathbf{W} \tag{5}$$

where $\mathbf{K}_S$ is the dynamic stiffness matrix of the layered ground corresponding to the interaction nodes.

A similar relation can be established by considering the equations of motion of the embankment. If the dynamic stiffness matrix of the embankment beam system is denoted by $\mathbf{K}_B$, and the vector of nodal motions is denoted by $\mathbf{U}$, one can write

$$\mathbf{F} - \mathbf{P} = \mathbf{K}_B \cdot \mathbf{U} \tag{6}$$

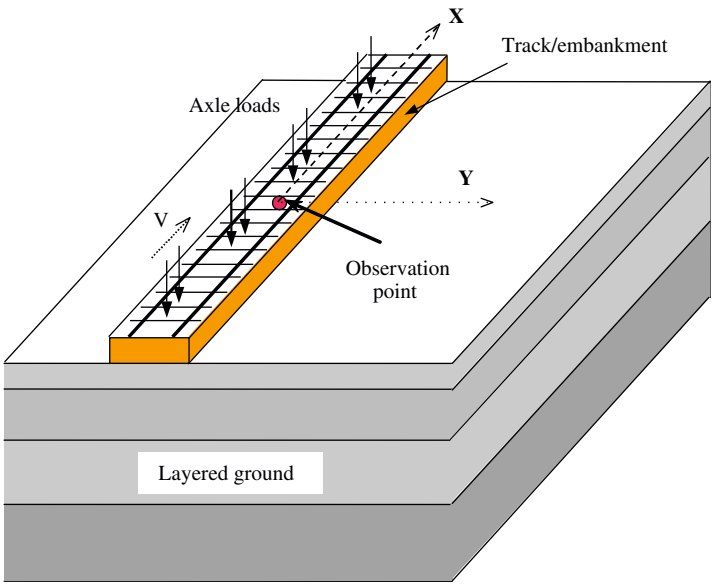

Fig. 3. Key features of simulation model in *VibTrain*.

where **F** is the vector of applied forces. The matrix $\mathbf{K}_B$ is assembled from the stiffness matrix $\mathbf{K}^i$ and consistent mass matrix $\mathbf{M}^i$ of a generic element I:

$$\mathbf{K}_B^i = \mathbf{K}^i - \omega^2 \mathbf{M}^i \tag{7}$$

The stiffness matrix $\mathbf{K}^i$ is calculated from the bending stiffness of a rectangular beam (embankment) $EI=Ebh^3/12$ where b and h are the average width and height and E is the average modulus of the embankment (e.g. [23]).

Finally, imposing displacement compatibility (**U**=**W**) and eliminating the interaction force vector from Eqs. (5) and (6), one obtains

$$\mathbf{F} = (\mathbf{K}_S + \mathbf{K}_B)\mathbf{U} \tag{8}$$

Essential to the above formulation is the implementation of a routine for the derivation of the Green's functions. In *VibTrain*, Green's functions for disk loads in layered media proposed by Kausel and Roësset [24] have been used. The radius of the disk load is taken such that the area of the disk is equal to the contact area at the embankment–ground interface between two adjacent nodes. The solution technique by Kausel and Roësset is based on the application of Fourier and Hankel transforms to the wave equations in each layer to reduce them to a series of ordinary differential equations. These equations are solved by the imposition of the appropriate stress and kinematic boundary conditions at layer interfaces and the free surface. Green's functions are finally evaluated by applying the appropriate inverse Hankel transforms. As an example, the vertical response due to a disk load with radius R at a distance r can be expressed as

$$u_Z(r,z) = \frac{1}{\pi}\int_0^\infty \overline{u}_2 J_0(kr)\frac{J_1(kR)}{kR}k\,dk \tag{9}$$

where J_0 and J_1 are the zero order and first order Bessel functions of the first kind, respectively, $\overline{u}_2$ is the vertical component of the Hankel transformed displacement and k is the wavenumber associated with the wavelength λ as $k=2\pi/\lambda$.

To account for the distribution of the axle loads on the embankment, the rails are modelled as separate beams on elastic foundation in the spirit of the conventional Zimmermann method. For this purpose, a finite element model of the rails is added to the finite element representation of the embankment–ground system (Eq. (8)) through discrete springs at the location of the sleepers.

Fig. 4 shows a schematic representation of this model. The figure shows the part of embankment directly under a sleeper. The stiffness of this element, identified in the following as Zimmermann's modulus *BK*1, represents the foundation modulus of the rails on the embankment and is derived from the stiffness of the embankment column directly under the sleeper. The vertical stiffness of this element, assuming an effective length of 1 m for the sleeper, is simply $EA/h=E(w+h/2)/h$ where E is the average elastic modulus of the embankment; the term $(w+h/2)$ represents the average width of the embankment column under the sleeper. In case there are other structural elements beneath the rails such as rail or sleeper pads, spring elements can be considered in series with the Zimmermann spring as shown in the

lower right part of Fig. 4. The equivalent stiffness for such a system of springs is calculated from

$$\frac{1}{K_{\text{equiv}}} = \sum_{i=1}^{n} \frac{1}{k_i} \tag{10}$$

where k_i is the stiffness of the ith spring in the series and n is the total number of springs.

The computational details for these springs and the other input parameters required for the calculation of Green's functions are given in the next section.

The VibTrain software has been used and verified in other projects, e.g. [22]. For this project minor adjustments have been made in order to extract receptance results comparable with measurements. A confirmation of these adjustments has been made by comparing results from the simulation model with 'standstill' measurements from a well-known location in Sweden with soft soils—Ledsgård. Measurement at this site was not made with the RSMV, instead the old Swedish Track Loading Vehicle (TLV) [14] was used. The TLV is a rebuilt passenger car with vertical and lateral track loading capabilities through hydraulic jacks. Each jack (one lateral and two vertical) is capable of 150 kN at low frequencies (<2 Hz); and lower forces up to 200 Hz. A normal vertical dynamic test is to pre-load the track with f ex 90 kN on each rail and superimpose a dynamic sine-sweep with a much lower (f ex 10 kN) amplitude as to avoid too much influence from possible nonlinear characteristics of the track. The TLV is used at standstill, whilst the RSMV is used while rolling.

In Ledsgård, there are several layers of clay and organic clay with shear wave velocities between 40 and 100 m/s. Fig. 5 shows an example of simulation and measurement results, where the general agreement is good—the simulation software

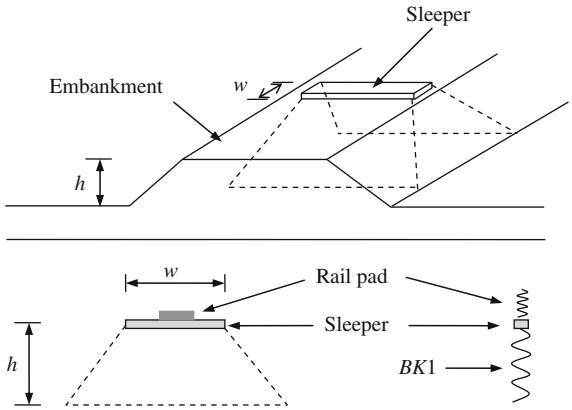

Fig. 4. Main elements of foundation modulus definition in VibTrain. The top part is showing the embankment section and the bottom part is showing part of the section from the side. Embankment thickness (h) and sleeper width (w) is indicated in both parts as well as the load carrying column through the embankment (dashed lines).

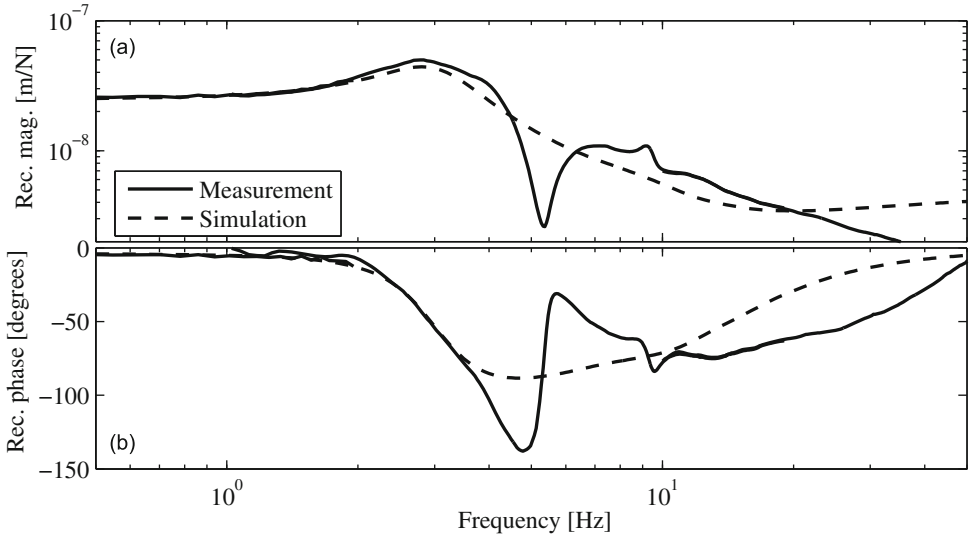

Fig. 5. Verification of the VibTrain model with measurement from the Ledsgård site south of Gothenburg, Sweden. Magnitude (a) and phase (b) of the vertical direct receptance for frequencies up to 50 Hz. The TLV used a static axle load of 2×90 kN.

captures the dynamic behaviour of the test site. The TLV excites the track during tests using hydraulic jacks in the middle of the car, directly coupled with the car body. Unfortunately the car body flexibility influences the measurements at some frequencies which can be seen around 5 Hz. At this frequency the TLV car body has its first resonance, meaning that low force excitation is transmitted to the track. The coherence function (not shown in the figure) is also low at this frequency indicating a poor transfer function estimate. At higher frequencies, the difference between simulation and measurement is probably due to model simplifications in the embankment (for instance the soft pad is not modelled as a unique spring). The measurements also show a smaller resonance at 9 Hz which is not captured by the simulation. This difference is not fully analysed, but probably the model separation in different homogenous layers is a simplification that leave out this resonance. However, the overall agreement is acceptable.

2.2. Parametric studies

The frequency response of the whole track subjected to excitation of unit vertical load on top of the rails is calculated for each specified frequency. For soft soils, all combinations of the input parameters in Table 3 have been simulated between 0.1 and 50 Hz, giving a total of $(3 \times 5 \times 4)$ 60 simulations. There is bedrock below the soil layer.

Case 'a' in Fig. 6 is used in the simulations; however the substructure often looks more like cases 'b' or 'c'. Therefore, when interpreting results from measurements it is preferable to use the terms equivalent embankment thickness (h), equivalent layer thickness (H) and equivalent shear wave velocity (c_s). The equivalent thicknesses (h, H) are indicated in Fig. 6 and equivalent shear wave velocity is the shear wave velocity of one single homogenous layer even though there are several layers. The parametric study has been kept simple since there are numerous combinations of these parameters. However, the basic behaviour may still be studied.

In addition, moraine-type subsoil was simulated for a few reference cases, but almost no resonance behaviour was found below 50 Hz. Table 4 presents the material input parameters for the different soils. The damping ratio in the table refers to the hysteretic damping in the soil. Damping depends on the induced shear strain in the soil and is therefore dependent on the applied load magnitude. For low shear strains, the damping ratio is typically in the range 1–2%. For the top soil layers closer to the loading and with the typical shear strains in these layers, one would expect a damping ratio in the range 3–4%. In practice, however, the damping has only a minor effect on the results because most of the soil damping

Table 3
Values used in parametric study.

Input parameter	Value
Shear wave velocity c_s (m/s)	40, 60, 80
Thickness of clay layer H (m)	1, 2, 4, 8, 16
Embankment thickness h (m)	0.35, 1, 2, 4

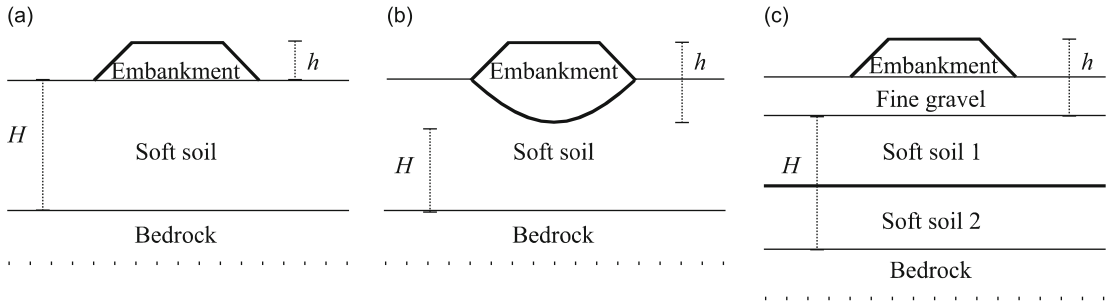

Fig. 6. Three different cases of substructure: (a) the ideal simulation case, (b) embankment/ballast intrusion in the soft soil layer (ballast pocket) and (c) several layers where the soft soils are deeper in the substructure.

Table 4
Subsoil parameter data.

Material	S-wave velocity (m/s)	Density (kg/m^3)	Damping ratio	Poisson's ratio
Soft clay	40	1500	0.06	0.49
Medium clay	60	1600	0.05	0.44
Normal clay	80	1700	0.04	0.40
Moraine	400	1900	0.02	0.30
Bedrock	1500	2300	0.02	0.30

comes from the radiation of the waves into the far field, the so-called radiation or geometric damping. The radiation damping is accounted for automatically by Green's functions formulation outlined in Section 2.1.

The model input parameters for the embankment are partly described in the previous section:

EI is the bending stiffness of the embankment (N m^2). *EI1* is the rail bending stiffness (N m^2) (6.42 MN m^2 in the simulations for UIC60 rail); *BK1* is the foundation modulus for rail on the embankment (N/m^2); *EM* is the mass of embankment (kg/m); *RP* is the radius of disk load for Green's function (not less than half the sleeper distance) (m).

These quantities are given by

$$EI = \frac{Ebh^3}{12} \tag{11}$$

$$BK1 = E\frac{w+h/2}{h} \tag{12}$$

$$EM = \rho hb \tag{13}$$

$$RP = 0.65\frac{h}{2} \text{ but } RP \geq 0.325 \tag{14}$$

where E is the average modulus of embankment material (160 MPa in simulations); h is the thickness of embankment; b is the mean width of embankment; w is the width of sleeper (0.15 m); ρ is the density of embankment material (1900 kg/m^3).

Embankment input parameters used in the simulations can be found in Table 5. A damping ratio of 6% was used for the embankment, although this value has only a minor effect on results, as discussed above. If the simulations are affected by numerical noise due to the wave reflections from the embankment boundary, one could reduce such artefacts by assigning larger damping values to the embankment.

Results from the simulations are given as track receptances. An example is shown in Fig. 7.

It is observed from these simulation results that the respective magnitude peak and phase shift at resonance, has a different shape for different simulations. Therefore the derivatives with respect to frequency may be used to evaluate this. These have been calculated for all simulations with an example in Fig. 8. The derivative of phase is also called group delay and is a measure of the time delay at different frequencies in system theory [25]. Note in Fig. 8b that the group delay and frequency for minimum group delay decreases with increased embankment thickness.

Table 5
Embankment and foundation modulus parameter data.

h (m)	b (m)	EI (MNm^2)	RP (m)	EM (kg/m)	$BK1$ (MPa)
0.35	3.7	2.14	0.325	2492	149
1	4.2	56.1	0.325	7994	104
2	4.9	524	0.65	18674	92
4	6.3	5400	1.3	48096	86

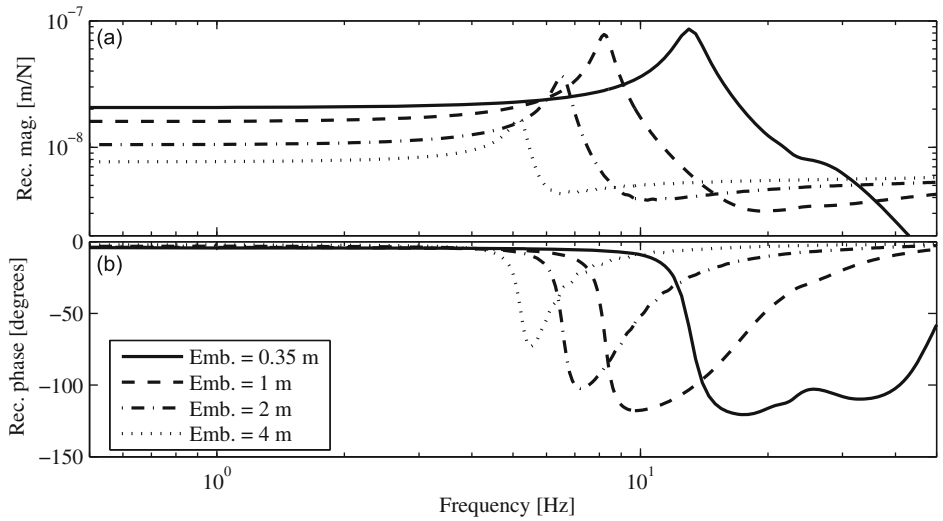

Fig. 7. Example from simulations with different embankment thickness on top of a clay layer (c_s=80 m/s, H=2 m): (a) receptance magnitude and (b) receptance phase.

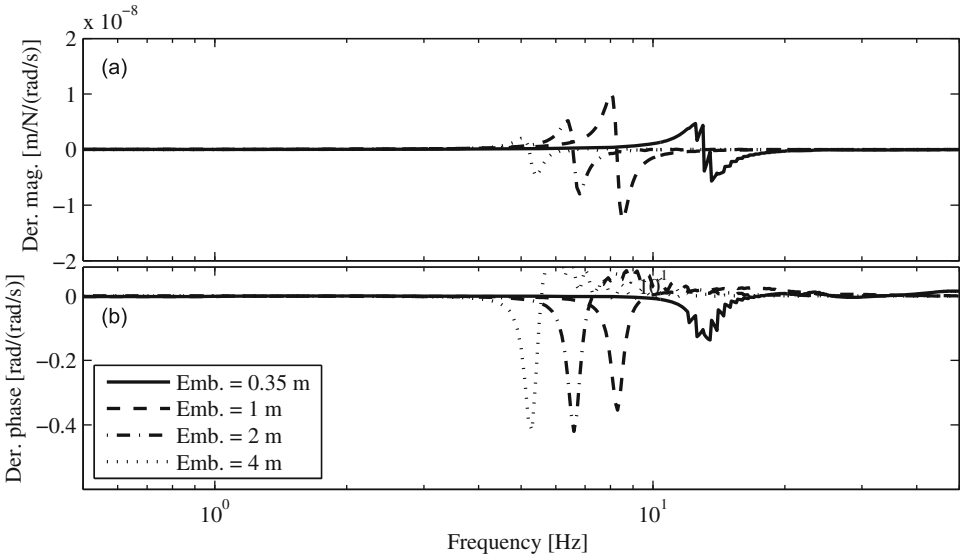

Fig. 8. Example from simulations with different embankment thickness on top of a clay layer (c_s=80 m/s, H=2 m): (a) derivative of receptance magnitude and (b) derivative of receptance phase (group delay).

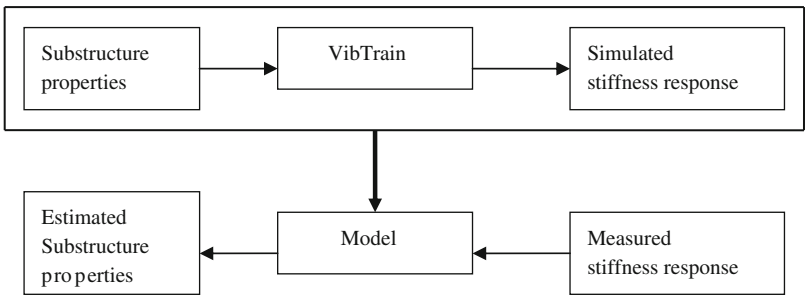

Fig. 9. Description of reference simulations to build model (upper part) and estimation of substructure properties from stiffness measurements (lower part).

3. Identification of substructure properties from simulations

The simulation results of Section 2 are represented by the upper part of Fig. 9. The core part of the research is to find patterns in the simulations that correspond to the parameters which were varied, building a model as in the lower part of Fig. 9. This will enable the use of stiffness measurements to estimate substructure properties. There are numerous ways to accomplish this, from simple linear relationships to more advanced techniques of pattern recognition [26]. In this study, one basic method (multiple regression) and two more advanced methods (Neural Networks and Relevance Vector Machine) has been used.

Using a model built from simulation on measured data can be relatively complicated. The simulations are based on simplified assumptions, and the measurements contain various uncertainties. Therefore another set of models based directly on measurement data, collected from GPR-measurements and information from boreholes, is also built. The lower part of Fig. 9 can describe these models as well.

Validation of the models is essential. For the models based on VibTrain simulation, every fifth simulation is used only for validation and not to build the model. For the models based on measured data, two data sets are used with accompanying models. Cross-validation is used to ensure correct validation.

3.1. *Identification by use of reference simulations*

The first step to build a pattern recognition model is to extract useable information (features) from measurements and/or simulations. This is often referred to as feature extraction. The main reason for using features is that pattern recognition techniques generally cannot handle dynamic behaviour. For this study all simulation and measurements are pre-processed by calculating track receptance. From the track receptance a number of different features are defined and saved for use in the pattern recognition models. In order to capture the low frequency soil dynamics properly, most of the features

describes the resonance behaviour of the receptance function. Eleven different features have been extracted from the simulated and measured receptances as listed in Table 6. As an example, each receptance is searched for a resonance. The resonance frequency is stored as feature number 3; the receptance magnitude at this frequency is stored as feature number 2 and the phase at the resonance is stored as feature number 10.

Firstly, the linear relationship of each feature to the varied parameters (Table 3) was investigated. An example for the minimum phase (feature 4 in Table 6) is given in Fig. 10.

None of the features could resolve a substructure property alone; therefore several features were combined. A two-dimensional example is shown in Fig. 11. Different embankment thicknesses are clustered in different regions in the figure, making it possible to estimate the embankment thickness from the two chosen features.

All twelve features listed in Table 6 have been tested in different combinations with different model techniques, i.e. Multiple Linear Regression (MLR), Neural Networks (NN) and Relevance Vector Machine (RVM). However, the study has

Table 6
Extracted features from simulations.

1	Static magnitude of receptance
2	Receptance magnitude at resonance
3	Resonance frequency
4	Minimum phase
5	Frequency at minimum phase
6	Minimum derivative of magnitude receptance
7	Frequency of max derivative of magnitude receptance
8	Minimum derivative of receptance phase
9	Frequency of minimum derivative of receptance phase
10	Minimum phase at first resonance
11	Frequency at minimum phase at first resonance
12	Relation of max and min receptance magnitude

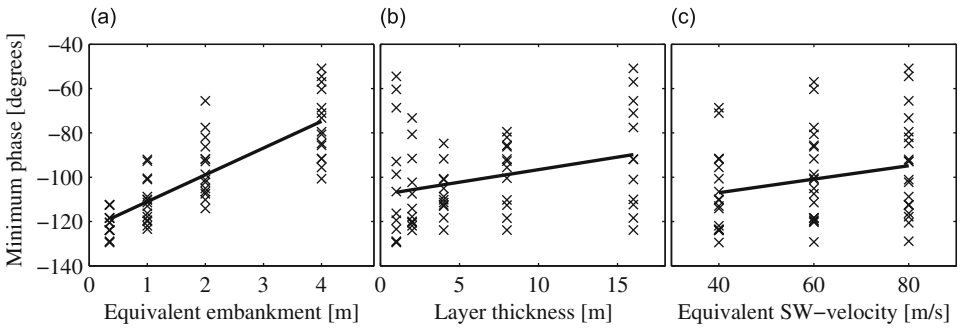

Fig. 10. Linear relationship between the feature minimum phase and substructure properties (the solid line is the least square estimate). Each cross represents a simulation of Table 3: (a) embankment thickness, (b) thickness of clay layer and (c) shear wave velocity.

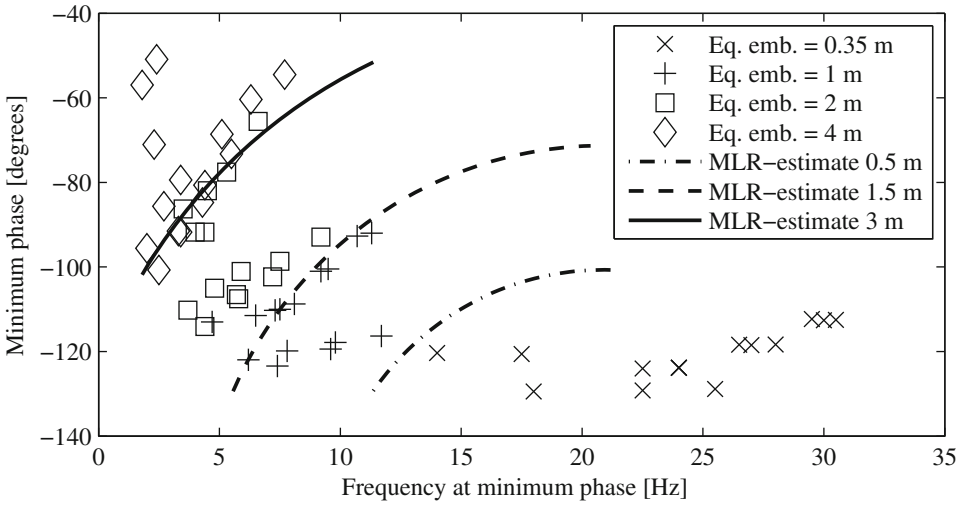

Fig. 11. Simulation results from two features (minimum phase and frequency at minimum phase) and corresponding estimation of embankment thickness. The multiple linear regression (MLR) estimation is calculated from second order polynomials of both features.

shown that most of the information is visible in features 3–5. There was no significant improvement by adding any of the other features which indicates a high degree of correlation between the chosen features of Table 6.

All 60 simulations and their corresponding value calculated with MLR-models from features 3–5 are shown in Fig. 12. It can be seen that embankment thickness and soil layer thickness give reasonable estimates, whilst shear wave velocity does not.

Neural Networks (NN) has been widely used for both regression and classification problems during recent decades. It is basically a way of combining linear (w_{ij}) combinations of input parameters and nonlinear transformations ($h(a_j)$) (symbols corresponding to Eq. (15)). This procedure is repeated in several steps, forming a *layer* for each step. Normally two steps are used as described in Eq. (15). During training of a Neural Network, all variables affecting both the linear and nonlinear behaviour are adjusted, making it possible to mimic complex relationships. An introduction is given in [26]. A diagram of a two-layer network is shown in Fig. 13 with symbols and subscripts corresponding to

$$y_k = h\left(\sum_{j-0}^{M} w_{kj}^{(2)} h\left(\sum_{i-1}^{D} w_{ji}^{(1)} x_i\right)\right) \tag{15}$$

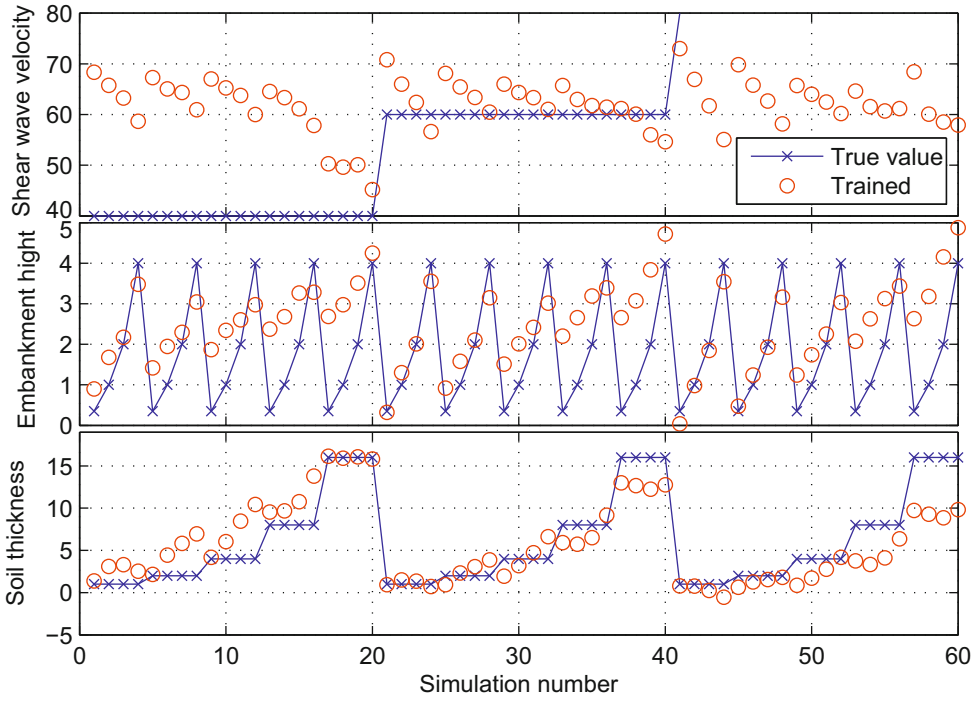

Fig. 12. All simulations and corresponding result from multiple linear regression based on features 3–5.

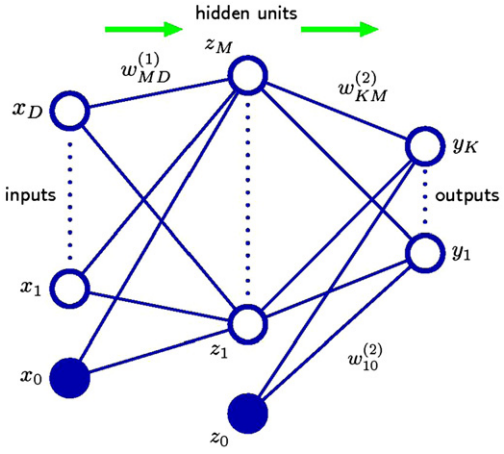

Fig. 13. Network diagram of a two-layer Neural Network (after Fig. 5.1 in [26]).

The software Netlab [27] was used for this application. A two-layer feed-forward network was trained and the number of so-called hidden units (M in Eq. (15) and Fig. 13) in the network was varied between 5 and 30. The best results were achieved for around 10 hidden units. Results are shown in Fig. 14.

Estimates of embankment thickness are here very good and predictions of soil thickness are acceptable; however shear wave velocities are harder to estimate, though better than MLR.

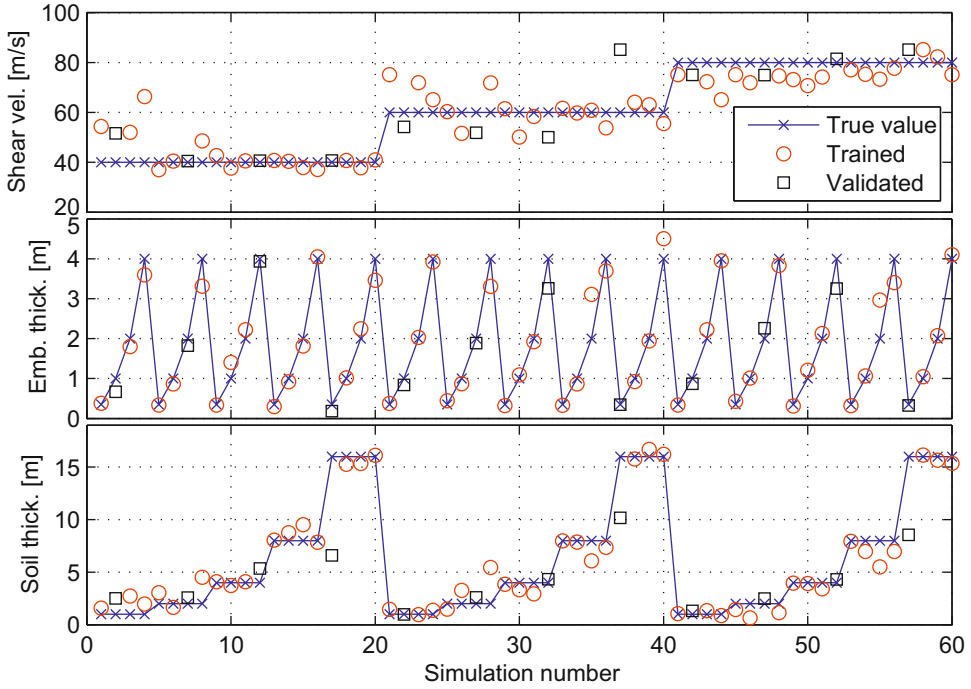

Fig. 14. All simulations and corresponding results from Neural Network analysis.

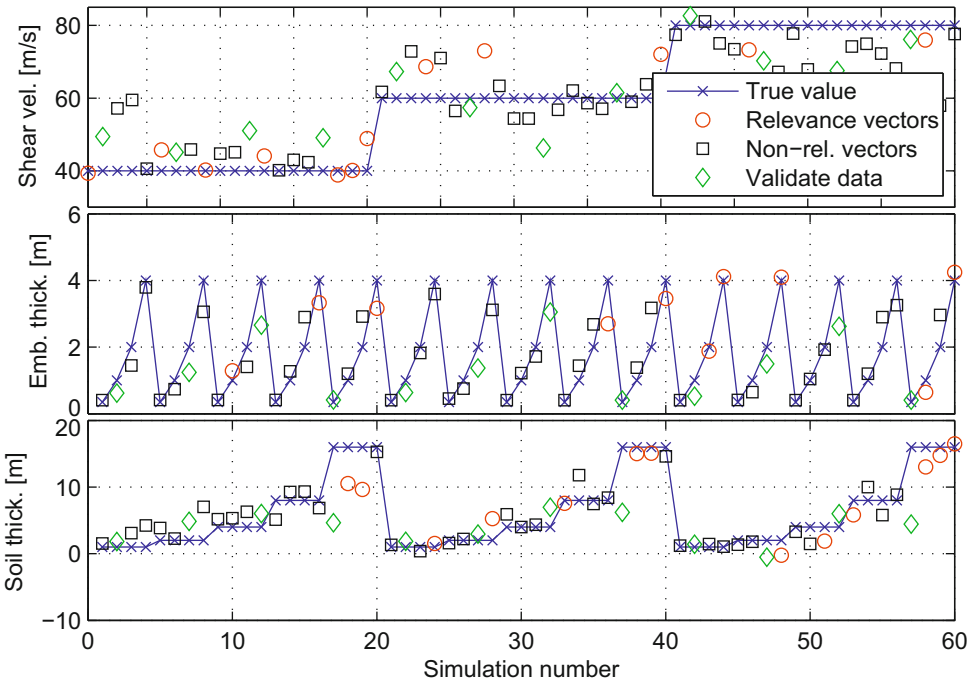

Fig. 15. All simulations and corresponding result from Relevance Vector Machine (RVM).

Table 7
Standard deviation of the error based on validated data for different methods.

Method	Embankment thickness (m)	Soil thickness (m)	Shear wave velocity (m/s)
MLR	0.92	2.8	16.6
NN	0.16	1.5	13.9
RVM	0.20	4.8	15.8

The third method tested is the Relevance Vector Machine (RVM). This method is based on the selection of a number of basis functions (different kinds of kernels) from the training data. These basis functions are saved and incorporated in the model. The new data is then compared with the basis functions and depending on the distance to the different basis functions, the estimate is calculated. RVM is built with a Bayesian formulation and includes a prior probability distribution of the parameters to be estimated. By this approach, model over-fitting is avoided and both robust and sparse models may be accomplished. RVM was first proposed by Tipping [28] and software for calculation is available at [29].

Fig. 15 illustrates results from the different simulations using RVM. Simulations that are used in the model are called relevance vectors and simulations that are used for training, but not stored in the model are called non-relevance vectors (cf. Fig. 15).

A comparison of results from the different methods (for validation data) is given in Table 7.

The main conclusion from these reference simulations and methods is that measurements from the RSMV (on soft soils) can provide good results for the embankment thickness, acceptable results for the soil thickness and more indicative information about shear wave velocity. The results so far are solely based on simulations. And based on these results, Neural Networks is the best method for all three substructure properties. A tougher test for the different methods will be to apply them on measured data, as will be accomplished in Section 4.

3.2. Identification by using GPR-measurements and boreholes

As stated in the beginning of Section 3, using models built from simulation on measured data is relatively complicated. The simulation results are not identical with the RSMV-measurements for a number of reasons, such as substructure variability, measurement uncertainties and evaluation techniques. In order to overcome some of these problems, models have also been developed by comparing RSMV-measurements with Ground Penetrating Radar (GPR) measurements. GPR-measurements on railway tracks are typically interpreted and calibrated so that the thickness of different layers can be estimated. Soft soils, however, can be harder to penetrate with GPR due to the high water content. The same methods described above have also been used for the GPR comparison. The main difference is that the true values for training the models are GPR layer thicknesses and borehole results instead of simulation parametric study.

Two sites are included in the study and one model is built for each site. One model is also developed using both sites. A cross-validation is performed by using the model from the first site to estimate layer thicknesses on the second site and vice-versa. No model was built for shear wave velocity, since no target measurements were available. Results for the two case studies are presented in Section 4.

GPR-measurements have some limitations needed to bear in mind in the following section. Firstly, GPR cannot penetrate clay (total reflection of electromagnetic waves on the clay surface) meaning only borehole results can be compared to the equivalent soil thickness when clay is present. Secondly, GPR-measurements use drillings for calibration of layer thicknesses, whereas the models from stiffness measurements do not. If a comparison is done between the methods proposed by this paper and GPR-measurements, the comparison will not be fair as GPR uses validation data (borehole information) to present layer thicknesses. However, as borehole information may be available, one possibility would be to extend the methodology proposed so that stiffness measurements and adherent models for substructure identification could also be calibrated. This is left for future research.

Normal values of GPR accuracy regarding ballast layer thickness is 4–8 cm [30].

4. Measurements and substructure identification: case studies

4.1. Description of measurement sites

4.1.1. Peat substructure near Björbo, Sweden

The track near Björbo, between Repbäcken and Vansbro, is old and in poor condition. There is mostly fine gravel or sand instead of broken stone ballast and long sections with soft subsoil, mostly peat. The track has wooden sleepers and jointed 43 kg/m rails. The RSMV excited the track with noise excitation between 3 and 20 Hz at a train speed of 5 km/h. The result in Fig. 16 is displayed as a 2-D surface with the stiffness phase and magnitude coded in grey scale. Black shall be interpreted as large phase delay/low stiffness and white as small phase delay/high stiffness (Fig. 17).

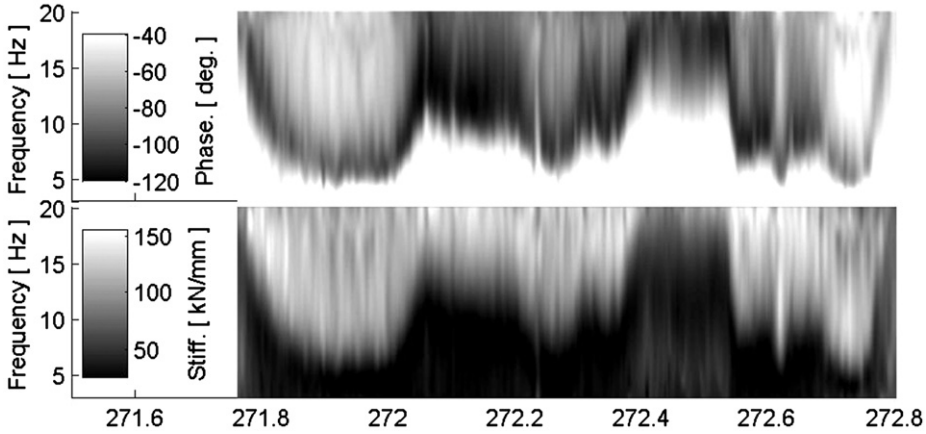

Fig. 16. Measurements of stiffness phase and magnitude with noise excitation at a speed of 5 km/h along 1 km of railway track (km 271.8–272.8) near Björbo.

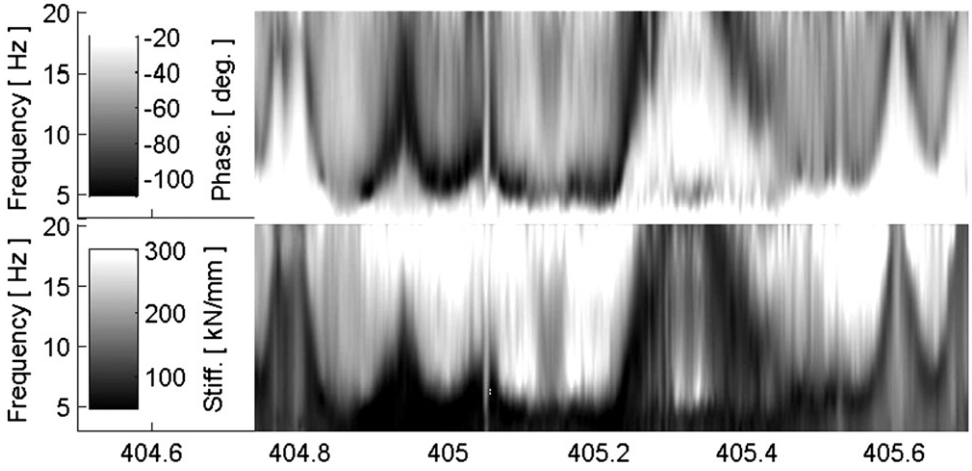

Fig. 17. Measurements of stiffness phase and magnitude with noise excitation at the speed of 5 km/h along 1 km of railway track (km 404.7–405.7) near Frövi.

It is rather easy to see the peat areas characterized by black areas with corresponding resonance behaviour. The stiffness resonance frequency varies, and this corresponds partially to changes in substructure properties as we try to estimate (cf. with result in Figs. 18 and 20).

4.1.2. Clay and peat substructure near Frövi, Sweden

The track between Ställdalen and Frövi is also old, but has been upgraded for an axle load of 25 metric tonnes. The upgrading focussed on embankment stability (loading berms, sheet pile walls) and drainage systems.

Several places where mud is visible in the vicinity of the sleeper (mud-pumping) have been found (km 405.25, 405.40 in this example) and the measurements were carried out to identify future borehole locations. The track has concrete sleepers and 50 kg/m rails. The RSMV excited the track with noise excitation between 3 and 20 Hz at a train speed of 5 km/h. The results are shown in Fig. 17. There are several cuttings surrounded by soft soil on this part of the track. These are visible in the lower figure as low stiffnesses at higher frequencies (km 404.8, 405.25–405.4, 405.6). There is a road crossing at km 405.05. After the cutting at km 404.8 there is peat subsoil to the next cutting at 405.25 (for the last part in combination with clay). After the cutting (from km 405.4) there is clay subsoil.

4.2. Identification of substructure parameters by models developed from simulation

The stiffness measurements have been interpreted according to the methodology outlined in Section 3. In Figs. 18 and 19, the models developed using *VibTrain* simulations have been used.

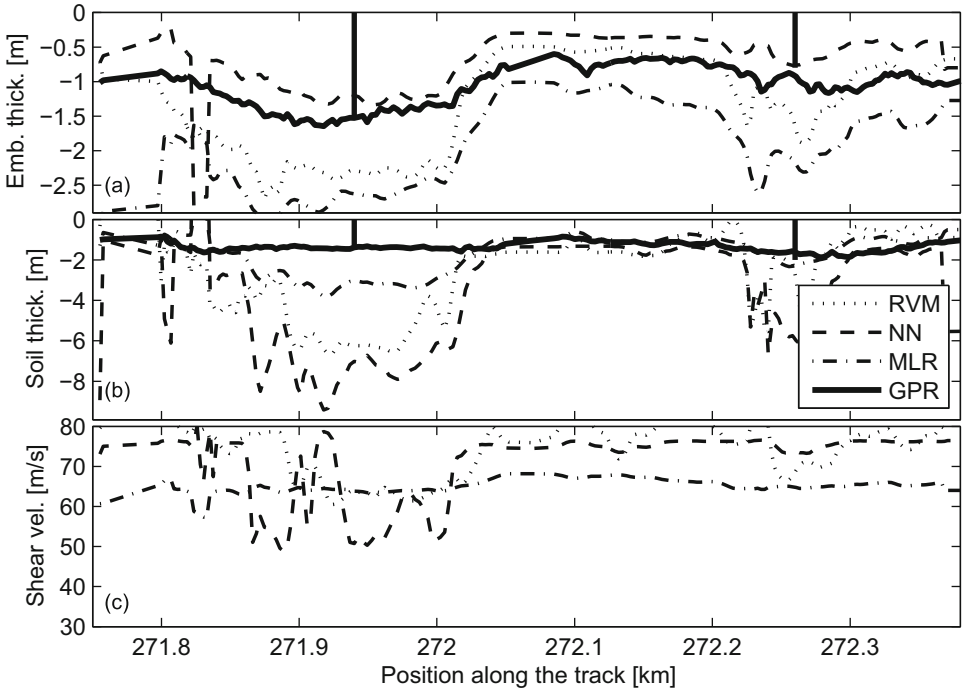

Fig. 18. Estimation from models based on simulations near Björbo: equivalent embankment thickness (a), thickness of soil layer (b) and equivalent shear wave velocity (c). GPR-measurement showed as thick solid line and borehole investigation as vertical bars in (a) and (b). RVM=Relevance Vector Machine, NN=Neural Network, MLR=Multiple Linear Regression and GPR=Ground Penetrating Radar—measured data.

The measurements from Björbo in Fig. 18 show that both the embankment and soil layer thicknesses vary along the track, which can also be seen from the GPR-measurements. The NN-model captures the embankment thickness variations. The RVM and MLR-models overestimate the embankment thickness, especially for thicknesses larger than 1.5 m. All models overestimate the magnitude of soil thickness; especially for thicknesses greater than 2 m (see Fig. 20 for better scaling). Unfortunately no comparison data are available for estimated shear wave velocity.

If the measurements from Frövi (Fig. 19) are considered, the estimation of equivalent embankment thickness shows good correlation with GPR-measurements and borehole data. For the first half, NN underestimates the equivalent embankment thickness and for the second half MLR and RVM overestimate the equivalent embankment thickness; otherwise the estimates are good. Close to the cuttings and at km 404.95 the equivalent embankment thickness is low. At these places there is most likely an increased risk of frost heave and thaw softening. Unsurprisingly, there is a known problem with track geometry at km 405.25 (not shown in this paper). Between km 405.3 and 405.35 there is no soft soil/resonance behaviour. Therefore the methods are not applicable and no results are shown.

As mentioned previously GPR-measurements cannot penetrate clay meaning that only borehole results can be compared to the equivalent soil thickness. The estimates diverge at some places; however the general agreement is reasonable.

As above, no comparison data are available for estimated shear wave velocity.

If the estimated results from Figs. 18 and 19 are compared with GPR, mean error and standard deviation can be calculated as is shown in Table 8. It can be seen that the results from the methods differ; there is not a one best method. RVM is the overall best method for embankment thickness and MLR is the best for soil thickness.

4.3. Identification of substructure parameters by models built from measurements

As described in Section 3.2, interpreted thicknesses from GPR-measurements have been used to develop models based directly on stiffness measurements. Several models have been built. In order to evaluate the performance properly, the models built on site 1 data are validated on site 2 and vice-verca. This process is normally referred to as cross-validation. In the results shown in Fig. 20, these models are referred to as "cross-val". The lines marked "all" represent models that include all data from both sites. Planned future work includes the development of a library of measurement sites in order to develop improved models.

The cross-validation of equivalent embankment thickness near Björbo (part a) overestimates the results, especially for thicker embankments (greater than 1 m). The same approach at near Frövi (part b), results in an underestimate of

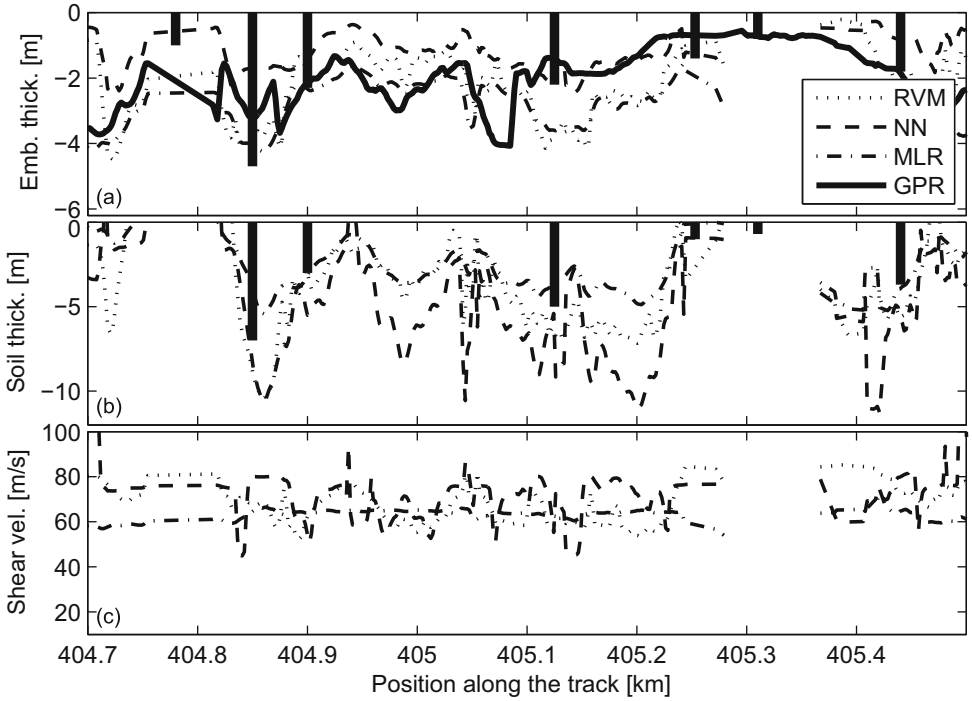

Fig. 19. Estimation from models based on simulations near Frövi: equivalent embankment thickness (a), thickness of soil layer (b) and equivalent shear wave velocity (c). GPR-measurement showed as thick solid line and borehole investigation as bars in (a) and (b). RVM=Relevance Vector Machine, NN=Neural Network, MLR=Multiple Linear Regression and GPR=Ground Penetrating Radar.

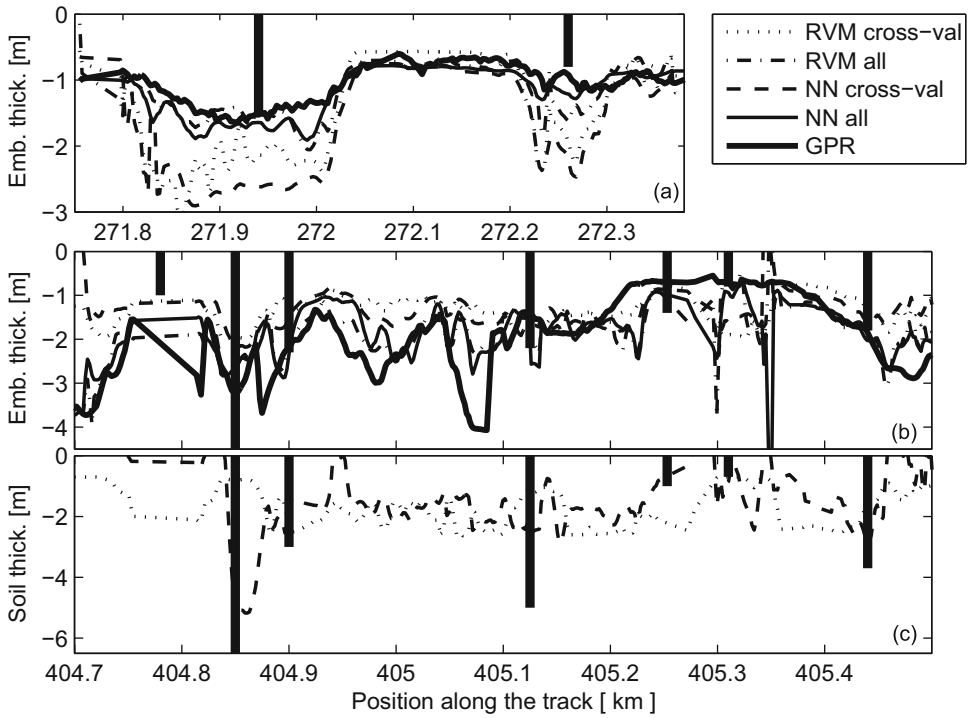

Fig. 20. Estimation from models developed using GPR-data: equivalent embankment thickness near Björbo (a), equivalent embankment thickness near Frövi (b) and thickness of soil layer near Frövi (c). GPR-measurement showed as thick solid line and bore-hole investigation as vertical bars. RVM=Relevance Vector Machine, NN=Neural Network and GPR=Ground Penetrating Radar.

Table 8
Mean error and standard deviation of the error based on validation with GPR-data for different methods developed from simulation.

Method	Embankment thickness Mean error/Standard deviation		Soil thickness Mean error/Standard deviation	
	Repbäcken (m)	Frövi (m)	Repbäcken (m)	Frövi
MLR	−0.99/0.46	−0.98/1.08	−0.33/0.98	–
NN	0.26/0.45	0.77/1.14	−2.26/2.90	–
RVM	−0.46/0.65	−0.35/1.39	−1.20/2.02	–

Table 9
Mean error and standard deviation of the error based on validation with GPR-data for different methods developed from measurements.

Method	Embankment thickness	
	Repbäcken (m)	Frövi (m)
NN cross-validation	−0.73/0.54	0.73/0.99
NN all data	−0.18/0.25	0.12/0.75
RVM cross-validation	−0.50/0.53	0.67/0.89
RVM all data	−0.17/0.29	0.15/0.67

equivalent embankment thickness. Both these deviations can partly be explained by the fact that we try to extrapolate values rather than interpolate.

The soil thickness cross-validation can only be performed for Frövi (part c) since the only GPR-data are for Björbo. It is difficult to draw clear conclusions when comparing only with borehole results. At some borehole locations there is good agreement, while others are poor. It is interesting to see that the NN-model indicates the deep clay layer at km 404.850 whereas the RVM-model does not.

If the estimated results from Fig. 20 are compared with GPR, mean error and standard deviation can be calculated as is shown in Table 9. It can be seen that the cross-validation results are slightly better with the RVM-model as compared with the NN-model. As expected there is a low error when using all data when building the models.

5. Conclusions and future work

With the newly developed Rolling Stiffness Measurement Vehicle (RSMV) it is possible to measure dynamic properties of railway tracks below 50 Hz while rolling. This paper has discussed how to interpret these measurements up to 20 Hz. Soft soils exhibit resonant behaviour at low frequencies. Parametric studies of soft soils using the software *VibTrain* have been performed to identify possibilities for characterising the response of soft soils using dynamic stiffness measurements. Several features have been extracted from the simulations and tested for correlation with substructure properties. No single feature could resolve a physical parameter for the substructure, but a combination of some features may be used to estimate substructure properties. It is shown that the equivalent embankment thickness and soil thickness may be estimated from dynamic stiffness measurements. Shear wave velocity is harder to estimate with any accuracy, although an indicative estimate can be obtained.

Comparing the results from pure simulation (Table 7) with models build from simulation used on real data (Table 8) shows that all three methods (MLR, NN, RVM) gives comparable results, though NN and RVM are slightly worse with real data as compared to pure simulation. Regarding soil thickness MLR gives remarkably good results for real data, which is probably due to that the measurement data from Repbäcken suits the model well. Data does not show much variation and it is not expected that the MLR will be the best choice for a more varied test place based on the results from pure simulation.

Models have also been developed directly from interpreted GPR-data with good results. Using this approach, it will be possible to build a library of stiffness–GPR relations to estimate track properties solely from stiffness measurements. Stiffness measurements and GPR-measurements are most often complementary and should be used together. However, this study shows that part of the GPR information is also present in dynamic stiffness measurement when considering soft soils.

Several methods for pattern recognition have been used in this paper. Depending on problem formulation, different models have performed best. For the pure simulation case, Neural Networks (NN) provided best results. When using the

models built from simulation on real data, Neural Network and Relevance Vector Machine (RVM) performed best for embankment thickness and multiple linear regression (MLR) provided best results for the estimate of soil thickness. Building models from measurement data (GPR and boreholes) and comparing the result with GPR-data gave comparable performance for the Neural Network and the Relevance Vector Machine.

In order to use these methods as standard techniques, it would be recommended to use a larger test set for building the models. As indicated above, a library of stiffness–GPR relations or even better stiffness–borehole relations for a variety of substructures is expected to produce better models. Also more simulations, with a larger variety of model parameters could improve practical use of the approach. A common extension in the use of pattern recognition methods, also suggested for future work, is the use of model-combination. This approach uses the fact that the error from different methods can be rather un-correlated and the combined estimate is often better.

References

[1] C. Esveld, *Modern Railway Track*, 2nd edition, MRT-Productions, Delft, 2001.
[2] E.T. Selig, J.M. Waters, *Track Geotechnology and Substructure Management*, Thomas Telford, London, 1994.
[3] A.M. Kaynia, D. Clouteau, Improved performance of ballasted tracks, in: A.G. Correia, Y. Momoya, F. Tatsuoka (Eds.), *Design and Construction of Pavements and Rail Tracks*, Taylor and Francis, London, UK, 2007 (Chapter 2).
[4] B. Paulsson, INNOTRACK – innovative track system – a unique approach of infrastructure managers and competitive track supply industry for developing the innovative products of the future, *Proceedings of IHHA Specialist Technical Session (STS)*, Kiruna, 11–13 June 2007.
[5] W. Wangqing, Z. Geming, Z. Kaiming, L. Lin, Development of inspection car for measuring railway track elasticity, *Proceedings from Sixth International Heavy Haul Conference*, Cape Town, 1997.
[6] D. Li, R. Thompson, S. Kalay, Development of continuous lateral and vertical track stiffness measurement techniques, *Proceedings from Railway Engineering Conference*, London, 2002.
[7] C. Norman, S. Farritor, R. Arnold, S.E.G. Elias, M. Fateh, M.E. Sibaie, Design of a system to measure track modulus from a moving railcar, *Proceedings from Railway Engineering Conference*, London, 2004.
[8] E. Berggren, Railway Track Stiffness—Dynamic Measurements and Evaluation for Efficient Maintenance, PhD Thesis, Royal Institute of Technology (KTH), Stockholm, 2009.
[9] S.L. Kramer, *Geotechnical Earthquake Engineering*, Prentice Hall, 1996 p. 261.
[10] A.S.J. Suiker, A.V. Metrikine, R. De Borst, Dynamic behaviour of a layer of discrete particles, Part 1: Analysis of body waves and eigenmodes, *Journal of Sound and Vibration* 240 (1) (2001).
[11] A.S.J. Suiker, A.V. Metrikine, R. De Borst, Dynamic behaviour of a layer of discrete particles, Part 2: Response to a uniformly moving, harmonically vibrating load, *Journal of Sound and Vibration* 240 (1) (2001).
[12] W.M. Zhai, K.Y. Wang, J.H. Lin, Modelling and experiment of railway ballast vibrations, *Journal of Sound and Vibration* 270 (4–5) (2004).
[13] B. Lichtberger, *The Homogenisation and Stabilisation of the Ballast Bed*, Rail Engineering International ed., no. 1993.
[14] A. Smekal, E. Berggren, Mitigation of track vibration at Ledsgård, Sweden, *Field Measurements Before and After Soil Improvement, Conference Proceedings of Structural Dynamics, EURODYN 2002*, Munich, 2002.
[15] D. Clouteau, G. Degrande, G. Lombaert, Some theoretical and numerical tools to model traffic induced vibrations, *Proceedings of the International Workshop Wave 2000*, Bochum, December 2000, 13–27, Balkema, Rotterdam.
[16] C.J.C. Jones, Use of numerical models to determine the effectiveness of anti-vibration systems for railways, *Proceedings of the ICE—Transport* 105 (1994) 43–51.
[17] C.J.C. Jones, X. Sheng, D.J. Thompson, Ground vibration from dynamic and quasi-static loads moving along a railway track on layered ground, *Proceedings of the International Workshop Wave 2000*, Bochum, December 2000, Balkema, Rotterdam, pp. 83–97.
[18] V.V. Krylov, Generations of ground vibrations from superfast trains, *Applied Acoustics* 44 (2) (1995) 149–164.
[19] C. Madshus, A.M. Kaynia, High-speed railway lines on soft ground: dynamic behaviour at critical train speed, *Journal of Sound and Vibration* 231 (3) (2000) 689–701.
[20] A.M. Kaynia, VibTrain: a computer code for numerical simulation of train-induced ground vibration, Report 514063-2, Norwegian Geotechnical Institute, September 1999.
[21] A.M. Kaynia, Measurement and prediction of ground vibration from railway traffic, *Proceedings of the 15th International Conference of Soil Mechanics and Geotechnical Engineering*, Istanbul, Turkey, August 27–31 2001, vol. 3, 2001, pp. 2105–2109.
[22] A.M. Kaynia, C. Madshus, P. Zackrisson, Ground vibration from high speed trains: prediction and countermeasure, *Journal of Geotechnical and Geoenvironmental Engineering, ASCE* 126 (6) (2000) 531–537.
[23] A.K. Chopra, *Dynamics of Structures*, Prentice Hall, New Jersey, 1995.
[24] E. Kausel, J.M. Roësset, Stiffness matrices for layered soils, *Bulletin of the Seismological Society of America* 71 (6) (1981) 1743–1761.
[25] F. Gustafsson, L. Ljung, M. Millnert, Signalbehandling (Digital Signal Processing), Studentlitteratur, Lund, 2000.
[26] C.M. Bishop, *Pattern Recognition and Machine Learning*, Springer, 2006.
[27] I. Nabney, Netlab software for Matlab, 〈http://www.ncrg.aston.ac.uk/netlab/index.php〉, 2003.
[28] M.E. Tipping, Sparse Bayesian learning and the Relevance Vector Machine, *Journal of Machine Learning Research* 1 (2001).
[29] M.E. Tipping, software for RVM, 〈http://www.miketipping.com/〉, 2006.
[30] J. Hugenschmidt, Railway track inspection using GPR, *Journal of Applied Geophysics* 43 (24) (2000) 147–155.